Structural and thermoelectric properties of AgSbTe$_2$-AgSbSe$_2$ pseudobinary system

K. T. Wojciechowski[*] and M. Schmidt

Faculty of Materials Science and Ceramics, AGH University of Science and Technology, Al. Mickiewicza 30, 30-059 Cracow, Poland
(Received 5 February 2009; revised manuscript received 15 April 2009; published 13 May 2009)

Structural properties of the AgSbTe$_2$-AgSbSe$_2$ pseudobinary system were examined using thermal analysis, scanning electron microscopy, and x-ray powder diffractometry. It was found that partial substitution of Te by Se atoms leads to stabilization of the cubic crystal structure of alloys. The electronic-transport properties of materials were measured in order to investigate carrier conduction, band-gap features, and thermoelectric properties. The undoped homogeneous solid solution exhibits extremely low thermal conductivity of 0.5 W m^{-1} K^{-1}, a very large positive Seebeck coefficient of about $400-600$ μV K^{-1} at room temperature, low carrier densities of $10^{16}-10^{18}$ cm^{-3}, and thermally activated conduction. The influence of alloying on thermal-conductivity mechanisms and electron properties was discussed. The highest experimental dimensionless figure of merit ZT of the undoped AgSbSe$_{0.25}$Te$_{1.75}$ sample is about 0.65 at a temperature of 520 K. The influence of doping on enhancement of thermoelectric properties of these materials was analyzed and optimal values of transport parameters were estimated.

I. INTRODUCTION

Known as narrow-gap semiconductors the ternary chalcogenides AgSbTe$_2$ and AgSbSe$_2$ feature very interesting optical and electronic properties. Both isostructural compounds crystallize in a disordered NaCl cubic structure (e.g., $Fm3m$) in which Ag and Sb randomly occupy the same crystallographic sublattice.[1–3] AgSbSe$_2$-based alloys are attractive as a switching medium for optical memories due to a reversible amorphous to crystalline-state transition.[4–8] Cubic AgSbTe$_2$ is recognized as a very promising p-type thermoelectric material for thermal energy conversion at the 500–800 K temperature range.

The effectiveness of thermoelectric materials for energy conversion is usually assessed by their dimensionless thermoelectric figure of merit ZT,

$$ZT = \alpha^2 \sigma \lambda^{-1} T, \tag{1}$$

where T is the temperature, α is the Seebeck coefficient, λ is the thermal conductivity, and σ is the electrical conductivity of a material. The AgSbTe$_2$ alloys with GeTe (so-called TAGS) with maximum value of $ZT_{max}=1.5$ at 750 K were considered the best TE materials for quite a long time.[9] Recently discovered PbTe alloys with AgSbTe$_2$ feature $ZT_{max}=2.2$ at 800 K which is the highest noticed figure of merit for bulk thermoelectric materials.[10] However, the application of those alloys seems to be limited as due to their thermodynamic instability and inhomogeneity they lose their excellent thermoelectric properties during a long-term annealing at high temperatures. Chen *et al.*[11] showed that PbTe-AgSbTe$_2$ alloys are, in fact, a multiphase on the scale of millimeters despite appearing homogeneous by x-ray diffraction and routine electron microscopy. Using a scanning Seebeck microprobe, they found a significant variation in Seebeck coefficient α including both n-type and p-type behaviors in the same sample. Inhomogeneous composition of materials leads to a significant decrease in the Seebeck coefficient by the circulating-current effect between p- and n-type grains of material.

The complicated behavior of AgSbTe$_2$-based materials can be a result of the complex nature of this compound which is also renowned for its difficulties in preparation and unstable chemical and physical properties. It has been noticed by many authors that single-crystalline and polycrystalline samples of AgSbTe$_2$, both prepared in standard conditions[12–15,17] as well as at high pressure,[18] have small amounts of precipitations of Sb$_2$Te$_3$, Ag$_2$Te, and other phases. Despite the fact that the inclusions in the measured specimens quite often present in quantities too small to be detected in x-ray patterns they affect the measured physical properties.

Thermal-analysis investigations of stoichiometric AgSbTe$_2$ indicate that it does not melt congruently.[12–15] From pseudobinary phase diagram[19] one can conclude that existing at high temperatures stoichiometric cubic AgSbTe$_2$ compound is unstable and decomposes below 633 K to Ag$_2$Te and Sb$_2$Te$_3$. However, it was not confirmed by further investigations of other authors. Extended elaborations of Sb$_2$Te$_3$-Ag$_2$Te and Sb$_2$Te$_3$-Ag$_2$Te-Te phase diagrams confirm that the thermodynamically stable compound with stoichiometric composition of AgSbTe$_2$, in fact, does not exist.[12–16] Marin-Ayral *et al.*[15] showed that in the temperature range from 300 to 817 K, the closest stable phase β of a cubic AgSbTe$_2$ structure has a real chemical composition of Ag$_{19}$Sb$_{29}$Te$_{52}$. This phase displays the behavior of solid solution with a narrow homogeneity range (42–44 at. % of Ag$_2$Te). However, in another paper[17] the very same authors reported that the received single-crystalline samples of this material have shown variations in their physical properties resulting from the existence of microfluctuations in the chemical composition.

Unlike the AgSbTe$_2$, its related phase-cubic AgSbSe$_2$ seems to have stoichiometric composition and does not exhibit visible first-order phase transitions up to the melting point at 883 K. It also demonstrates very promising properties such as large Seebeck coefficient and extremely low thermal conductivity.[20] The electronic structure calculations for a disordered crystal structure as well as for ordered superstructures (approximants) of AgSbSe$_2$ and AgSbTe$_2$ con-

firm that both compounds have a very similar configuration of electronic bands indicating similar ground-state properties.[20–22] Depending on assumed type of ordering in theoretical models, the two materials are semiconductors with a very narrow band gap or semimetals with the Fermi level E_f shifted on the valence-bands edge, which explains their p-type sign of thermopower. $AgSbTe_2$ shows slightly higher density of states (DOS) value at Fermi level than $AgSbSe_2$, which is consistent with its much higher electrical conductivity σ.

We expect that the alloying of $AgSbTe_2$ with isoelectronic and isostructural $AgSbSe_2$ can allow stabilizing its structure and receiving homogeneous alloys in some range of compositions. On the other hand, we assume that the obtained materials should inherit good thermoelectric properties of both base compounds. Therefore the specific objectives of our experimental investigation are as follows: (a) the analysis of phase stability in $AgSbTe_2$-$AgSbSe_2$ pseudobinary system, (b) the measurements of transport properties of the obtained materials, and (c) the assessment of their thermoelectric figure of merit ZT_{max} for optimal concentration of current carriers.

FIG. 1. (Color online) XRD patterns of $AgSbSe_xTe_{2-x}$ samples (series 1). For comparison, XRD patterns of slowly and rapidly (marked with *) cooled $AgSbTe_2$ samples are presented.

II. EXPERIMENTAL DETAILS

We have prepared nine sets of samples with nominal composition of $AgSbSe_xTe_{2-x}$ (with $x = 0,00$ 0.25, 0.50, 0.75, 1.00, 1.25, 1.50, 1.75, and 2.00). Elements with purity of 99.99%, in form of small pieces, were closed in sealed quartz ampoules, covered inside with a thin layer of pyrolytical carbon. Synthesis was carried out for 1 h at temperature of 700 °C in a rocking furnace. At this temperature elements Te, Se, and Sb were melted and Ag was completely dissolved in the melt. After synthesis ampoules were slowly cooled down to room temperature (RT). Materials were ground and formed in cylindrical samples with a diameter of $d = 10$ mm by using hot-pressing method (graphite dies, argon atmosphere, $T_{max} = 410$ °C, $t = 15$ min, and $p = 30$ MPa). During cooling to RT the pressure was taken off. The samples were cut with a diamond saw and polished. For structural investigations two series of samples were prepared: (a) slowly cooled down with the rate of 1 K min^{-1} and (b) rapidly cooled down with the rate >500 K min^{-1}. For electrical measurements samples with the cylindrical shape of 15 mm in height and 10 mm in diameter were used.

Materials were characterized by x-ray diffraction (X'Pert Philips diffractometer, with filtered Cu K$_\alpha$ radiation) and scanning electron microscopy (JEOL JSM-840) with an electron-probe microanalysis apparatus. The lattice parameters were determined from the x-ray patterns by Rietveld refinement method. Thermal analysis of materials was done by applying a differential scanning calorimeter (DSC) (TA-Instruments DSC 2010). Mass densities were determined with the use of immersion technique with water as a liquid. Thermal conductivity was measured by two methods: laser-flash (Netzsch LFA 457) and the axial heat-flow method in which a specifically calibrated heat-flux sensor designed for measurements of very low thermal conductivities was applied.
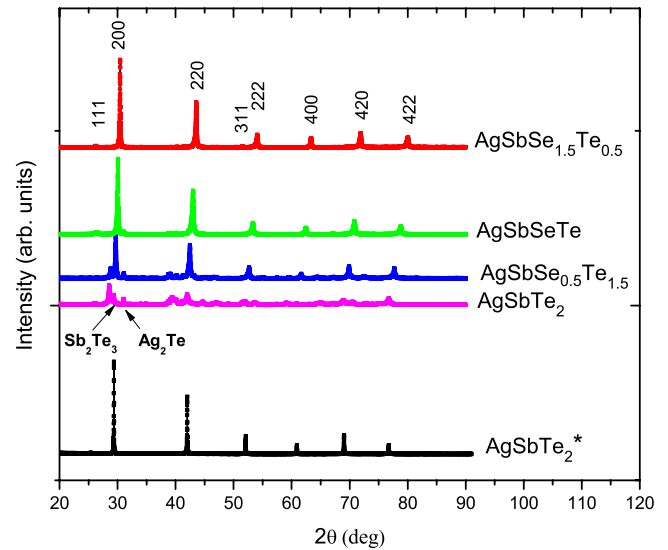
The Hall coefficient R_H was measured using low frequency (7 Hz) ac current of 50–100 mA/mm^2 in a constant magnetic field of 0.705 T at room temperature. Carrier concentrations were evaluated from the Hall coefficient R_H, assuming a Hall scattering factor A equal to 1.0.

III. RESULTS AND DISCUSSION

A. Structural and thermal analysis

Microstructure and phase composition of all $AgSbSe_xTe_{2-x}$ samples were characterized by using x-ray diffraction (XRD), scanning electron microscopy, and DSC techniques. The x-ray diffraction analysis in Fig. 1 revealed that materials with composition parameter $0 \leq x < 1$ consist of the main phase with a cubic structure and a few other phases of which some were identified to be isostructural with Ag_2Te, Sb_2Te_3, and Ag_5Te_3. The amount of precipitations increases during annealing of materials in the temperature of about 600 K and during slow lowering of temperature after their synthesis.

For comparison, Fig. 1 shows the selected results of XRD investigations for slowly cooled samples (series 1) and rapidly cooled $AgSbTe_2$ material (series 2). It can be noticed that in the case of rapidly cooled $AgSbTe_2$ the amount of precipitations is practically invisible (less than 2%). However the amount of inclusions in the same material as well as in samples with composition $0 \leq x < 1$ greatly increases as a result of annealing. Microscopic investigations show the Widmanstätten-type microstructure of these samples with visible plate-shape precipitations noticed by others.[13,15]

The DSC analysis in Fig. 2 of a sample with nominal composition of $AgSbTe_2$ reveals the presence of an evident sharp endothermic peak with broad asymmetrical shoulders which suggest multifaceted character of phase transitions. The beginning of this peak is situated in the temperature of about 630 K. Therefore, it can be assigned to the melting
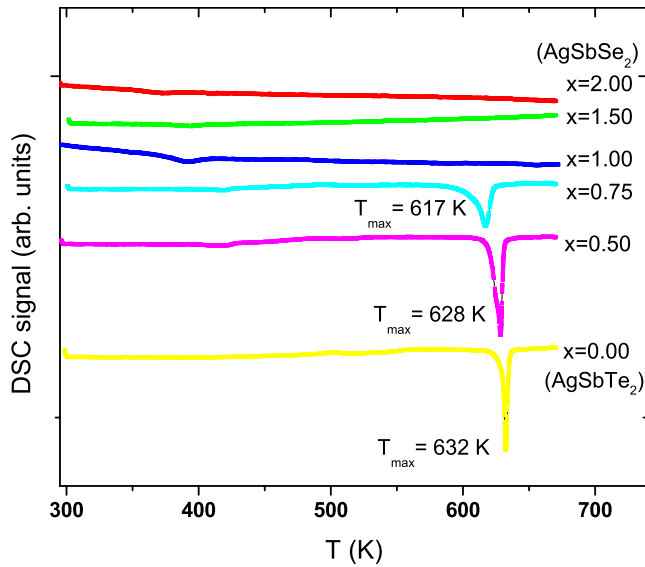
FIG. 2. (Color online) DSC curves of $AgSbSe_xTe_{2-x}$ samples (heating rate 5 deg min^{-1} and sample mass 20/60 mg).

FIG. 3. (Color online) Lattice parameter a vs composition x of $AgSbSe_xTe_{2-x}$ samples (estimated errors of regression-line coefficients are calculated at the significance level $p=0.05$).

point of eutectic with a nominal composition of $Ag_{0.35}Sb_{0.09}Te_{0.56}$ (633 K), as given in the ternary phase diagram of the Ag-Sb-Te system.[15]

The position of the peak maximum T_{max} moves in the direction of lower temperatures as a result of alloying with $AgSbSe_2$ for subsequent samples with the x parameter changing from 0 to 1 (Fig. 2). For samples with $x \geq 1$ this peak completely vanishes. The XRD analysis of the same samples shows no presence of any secondary phases (Fig. 1). Therefore, on the basis of the above observations we conclude that samples with composition changing from $AgSbTe_2$ to AgSbSeTe ($0 \leq x < 1$) are multiphased and samples with the amount of Se greater than Te are homogeneous solid solutions.

This result is consistent with an observed cell size a vs x relationship of the main cubic phase of the materials (Fig. 3). The statistical analysis (the parallelism test at a significance level $p=0.05$) confirmed the presence of two regions with almost linear dependences of cell size a versus a composition parameter x. Particularly, it should be noted that for the homogeneous solid solutions Vegard's law is very well carried out. We have expected that the materials in the area of homogeneity should have repeatable properties hence our successive investigations of physical properties were mostly focused on these samples.

B. Transport properties

Transport properties of obtained materials, both electrical and thermal conductivities as well as thermopower, are related to their microstructure. Figure 4 presents selected results of electrical conductivity measurements at 336, 407, and 507 K against chemical composition x. The highest conductance $\sigma = 3.3 \times 10^4$ S·m^{-1} at RT exhibits the sample with nominal composition of $AgSbTe_2$ which is comparable to the value of 1.5×10^4 S m^{-1} reported for single crystals.[23] Generally, samples with precipitations of secondary phases ex-
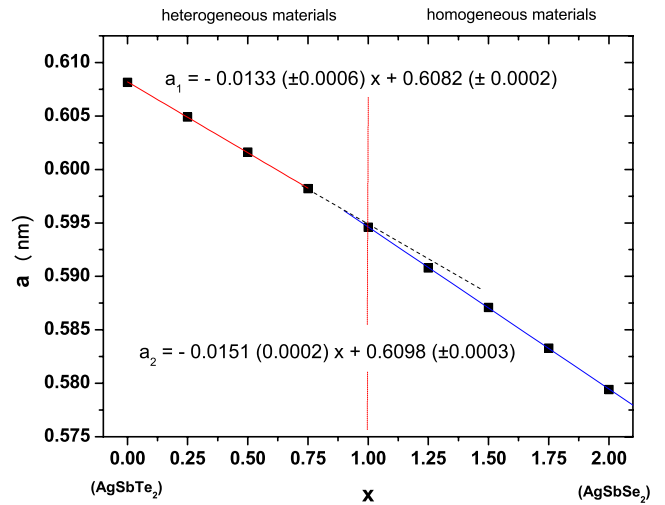
hibit much higher electrical conductivity than homogeneous materials and semimetallic or metallic behavior. Single-phased materials ($x \geq 1$) demonstrate semiconducting temperature dependence on electrical conductivity.

The Seebeck coefficient measurements were taken for all samples at temperature between 300 and 530 K. Thermopower measurements show that all samples exhibit resultant p-type sign of current carriers in the whole temperature range. $AgSbSe_xTe_{2-x}$ materials with composition parameter $x \geq 1$ have very high Seebeck coefficient α of about $500-600$ μV K^{-1}, which is about two to five times higher than the values for pure samples $AgSbSe_2$ and $AgSbTe_2$, respectively. The Seebeck coefficient of heterogeneous samples is lower than single-phased alloys (Fig. 5). All the samples produced, both homogeneous and heterogeneous, are dominantly p type, which can be due to presence of Ag vacancies,[15] or in case of inhomogeneous samples, mostly due to microstructural defects and precipitations.
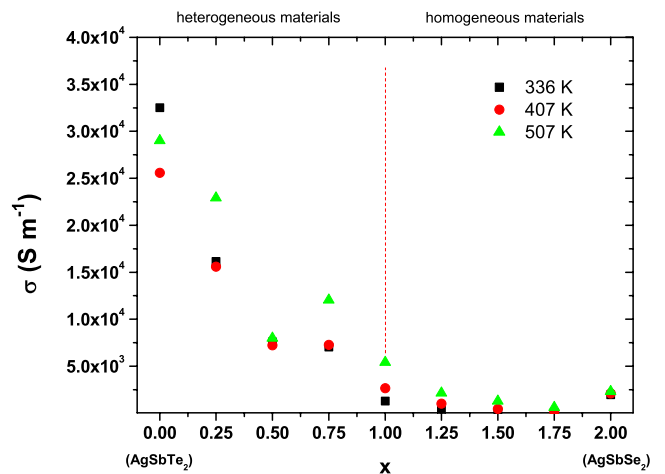

FIG. 4. (Color online) Variation in electrical conductivity σ with composition x of $AgSbSe_xTe_{2-x}$ materials at temperatures of 336, 407, and 507 K.
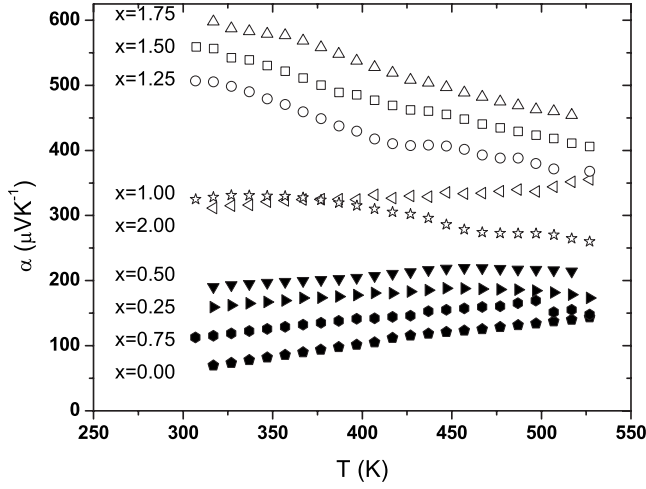
FIG. 5. Temperature dependence of the Seebeck coefficient of AgSbSe$_x$Te$_{2-x}$ (filled markers: heterogeneous materials; hollow markers: homogeneous materials).

Figure 6 displays temperature dependences of electrical conductivity in the Arrhenius plot. It can be observed that the base materials AgSbSe$_2$ and AgSbTe$_2$ have properties of narrow-band semiconductors. Estimated E_g values for these samples are about 0.09 and 0.03 eV, respectively. This result is consistent with previous measurements and with the results of band-structure calculations for both isostructural compounds pointing even to their semimetallic features.[20,22] Interestingly enough, that in case of homogeneous alloys ($x \geq 1$), temperature dependences of electrical conductivity indicate on their apparent thermally activated character ($E_g \sim 0.3/0.4$ eV) in the whole temperature range or partially, in high-temperature region ($T > 450$ K) for samples with smaller Se contents ($x < 1$). The evident semiconducting behavior of homogeneous materials ($x \geq 1$) is correlated with their very high thermopower values, which supports the above observations.
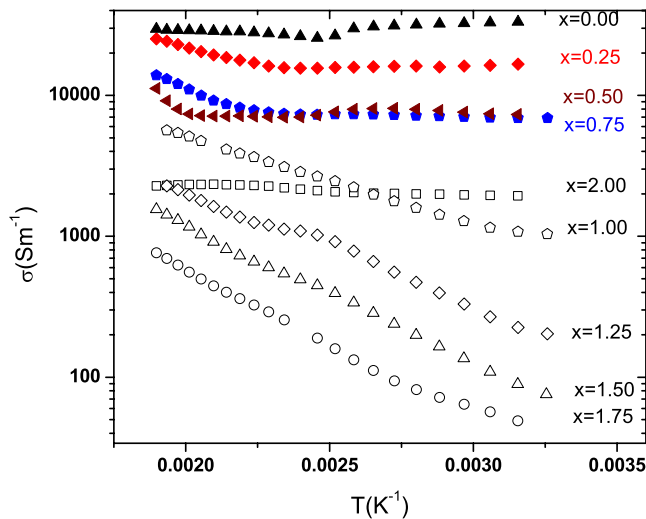

FIG. 6. (Color online) Temperature dependence of the electrical conductivity of AgSbSe$_x$Te$_{2-x}$ (filled markers: heterogeneous materials; hollow markers: homogeneous materials).

Semiconducting properties of the materials, obtained as a result of alloying of semimetallic AgSbSe$_2$ and AgSbTe$_2$ compounds, seem to be an unexpected outcome and cannot be explained as a simple consequence of substitution of Te by isoelectronic Se atoms. We believe that the occurrence of semiconducting properties indicates rather on structural changes (e.g., ordering in at least one of sublattices) as a result of alloying and thus subsequent changes in the electronic structure. This supposition is supported by our previous theoretical predictions pointing to a possibility of opening of a band gap in ordered AgSbSe$_2$ (e.g., $Fd3m$) (Ref. 20) as well as by the results of Hoang *et al.*[22] who showed a significant impact of the Ag or Sb ordering on the electronic structure of ternary chalcogenides in the neighborhood of E_f. However, in order to clarify this problem more advanced structural investigations are necessary.

The Seebeck coefficient and Hall carrier-concentration data were used to estimate the effective mass of carriers m^*, assuming a single-parabolic band model with acoustic phonon scattering ($r = -\frac{1}{2}$) as a predominant carrier scattering mechanism. In this model, the Seebeck coefficient α can be expressed as follows:

$$\alpha = -\frac{k_B}{e}\left(\frac{2F_1(\eta)}{F_0(\eta)} - \eta\right). \quad (2)$$

The carrier concentration n is

$$n = 4\pi\left(\frac{2m^* k_B T}{h^2}\right)^{3/2} F_{1/2}(\eta), \quad (3)$$

where k_B is the Boltzmann's constant, F_x is the Fermi integral of order x, m^* is the effective mass of carriers, and T is the absolute temperature. The reduced Fermi energies are given by $\eta = E_F/k_B T$.

At first, we calculated the reduced Fermi levels η from the experimental Seebeck coefficient data using Eq. (2). Then, the determined hole effective masses from Eq. (3) using the calculated reduced Fermi energies and the experimental Hall carrier-concentration values. Table I presents the results of computations for our materials at RT.

Inhomogeneous samples exhibit variable amounts of hole concentrations from 6.4×10^{18} to 1.8×10^{19} cm^{-3} and effective masses m^* of 0.21–0.85 of free-electron mass m_0. The effective mass $m^* = 0.21m_0$ determined for AgSbTe$_2$ can be related to the recent results of Jovovic and Heremans,[24] who measured the de Haas–van Alphen effect in single crystals with hole concentration of 5×10^{19} cm^{-3} and with the magnetic field oriented along the $\langle 111 \rangle$ axis. They confirmed the calculated complex valence-band structure composed of 12 half pockets located at the X points of the Brillouin zone, six with a density-of-states effective mass $m_{da} = 0.21m_0$ and six with $m_{db} = 0.55m_0$.[24] The determined total cyclotron-effective mass $m_d = 1.5 \pm 0.2m_0$ was larger than estimated by us value. The discrepancy can be a consequence of lower carrier concentration in our samples and due to applied methodology larger contribution of light hole effective mass in the final result.

TABLE I. Room-temperature physical parameters of samples with nominal composition of $AgSbSe_xTe_{2-x}$.

x	0.00	0.25	0.50	0.75	1.00	1.25	1.50	1.75	2.00
n [cm^{-3}]	1.0×10^{19}	9.1×10^{18}	1.8×10^{19}	6.4×10^{18}	2.8×10^{17}	1.8×10^{16}	1.2×10^{16}	1.3×10^{15}	
μ [cm^2 V^{-1} s^{-1}]	200	120	25	67	240	790	470	2400	
m_h/m_0	0.21	0.42	0.85	0.23	0.15	0.1	0.11	0.03	
E_g [eV]	0.03				0.24	0.32	0.38	0.39	0.09

Determined effective masses of majority carriers in homogenous alloys ($x \geq 1$) are correlated with their concentration (Table I). It can be observed that charge transport in samples with increasing Se content is dominated by lighter holes with very high mobility. However, assuming similarity of band structure of $AgSbSe_xTe_{2-x}$ alloys to $AgSbSe_2$ and $AgSbTe_2$ compounds,[20,21,24] one can expect that increasing of carrier concentration should move Fermi level toward flat bands corresponding to high effective masses.

C. Thermal conductivity

Thermal-conductivity measurements of the samples were performed with the use of two techniques: a precise steady-state heat-flow technique which was applied at room temperature and a pulsed laser-flash method for measurements in the temperature scope of 80–600 K. Within the limit of their accuracy both methods provided consistent experimental results.

Similarly to the results for electrical-transport properties, there are noticeable differences in properties of homogeneous and heterogeneous materials (Fig. 7). Thermal-conductivity values of single-phased solid solutions are generally more consistent and lower than for heterogeneous samples. The discrepancies are visible in particular for base compounds: $AgSbSe_2$ and $AgSbTe_2$. Thermal conductivity λ of $AgSbSe_2$ is about 0.6 W m K^{-1} and is comparable with

FIG. 7. (Color online) Variation in thermal conductivities λ, $\lambda_{latt.}$, and λ_{el} with composition x of $AgSbSe_xTe_{2-x}$ materials at RT (experimental error 5%).

previous findings,[25] however, thermal conductivity of $AgSbTe_2$ (0.82 W m K^{-1}) is significantly higher than values reported for single-crystalline $Ag_{19}Sb_{29}Te_{52}$ samples (0.61 W m^{-1} K^{-1}).[23] This difference as well as generally higher conductivities of heterogeneous materials in comparison with the remaining samples can be the effect of larger electronic contribution of thermal conductivity λ_{el}, caused by higher concentration of current carriers generated by, e.g., point defects and inclusions of secondary phases.

In order to explain the impact of the electronic contribution on thermal conductivity of materials, the Wiedemann-Franz-Lorenz law can be applied as

$$\lambda_{el} = LT\sigma, \tag{4}$$

where L is the Lorenz number, which may vary from 1.49×10^{-8} V^2 K^{-2} for nondegenerated semiconductors to 2.44×10^{-8} V^2 K^{-2} for metals and for strongly degenerated semiconductors. Depending on the composition, our materials behave as semiconductors or semimetals. For this reason, we determined the Lorenz number L and the electronic part of thermal conductivity with the use of Fermi-Dirac statistics as follows:

$$L = \frac{k_B^2}{e^2}\left[\frac{r + 7/2}{r + 3/2} \cdot \frac{F_{r+5/2}(\eta)}{F_{r+1/2}(\eta)} - \left\{ \frac{r + 5/2}{r + 3/2} \cdot \frac{F_{r+3/2}(\eta)}{F_{r+1/2}(\eta)} \right\}^2 \right] \tag{5}$$

assuming scattering factor $r = -1/2$.

The Fermi-level η values, which were used in the above calculations, alike those of carrier effective masses, were estimated with the use of absolute Seebeck coefficient α experimental data. The lattice conductivity $\lambda_{latt.}$ can be calculated by subtraction of the electronic component λ_{el} from the total thermal conductivity

$$\lambda_{latt.} = \lambda - \lambda_{el}. \tag{6}$$

The results of above calculations are presented in Fig. 7. Indeed, inhomogeneous samples reveal high-electronic part of thermal conductivity λ_{el} comprising about 20%–40% of total thermal conductivity λ. Homogeneous $AgSnSe_xTe_{2-x}$ ($1 < x < 2$) solid solutions have much lower electronic contribution, less than 1%. Almost all heat flux in these alloys is transported by the crystal lattice. It can also be noticed that the calculated lattice-thermal conductivity $\lambda_{latt.} = 0.61$ W m^{-1} K^{-1} for $AgSbTe_2$ is comparable to the value of 0.57 W m^{-1} K^{-1} and 0.68 W m^{-1} K^{-1} (Refs. 17 and 23) determined for single crystals with low concentration of current carriers.

In general, alloying of materials leads to the reduction of lattice-thermal conductivity $\lambda_{latt.}$ in comparison to the base

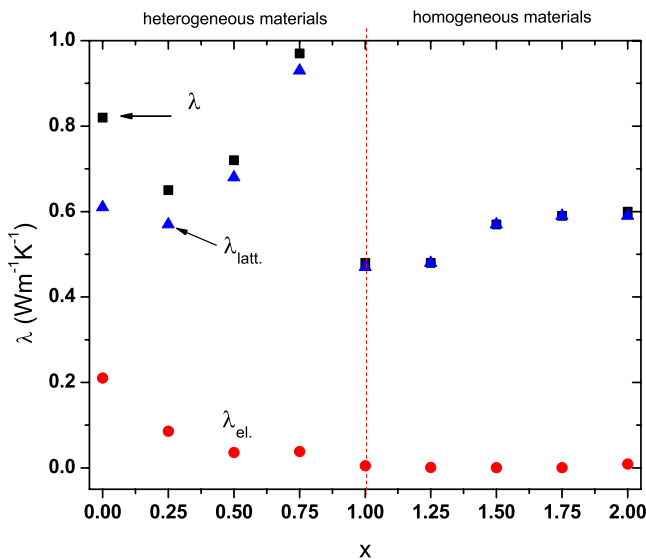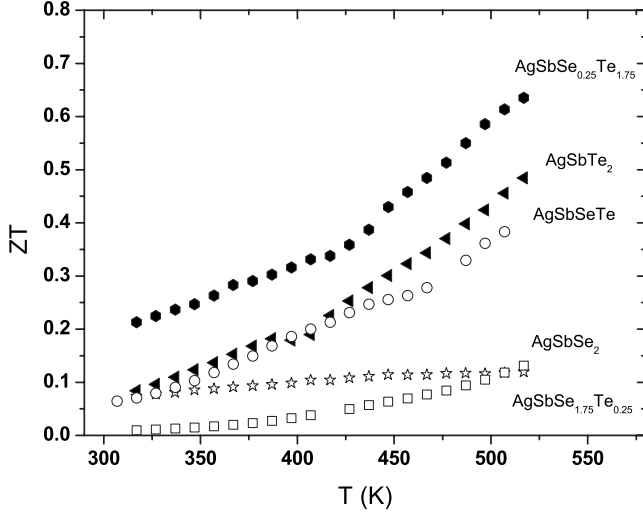FIG. 8. Temperature dependence of the thermoelectric figure of merit ZT of selected samples (filled markers: heterogeneous materials; hollow markers: homogeneous materials).
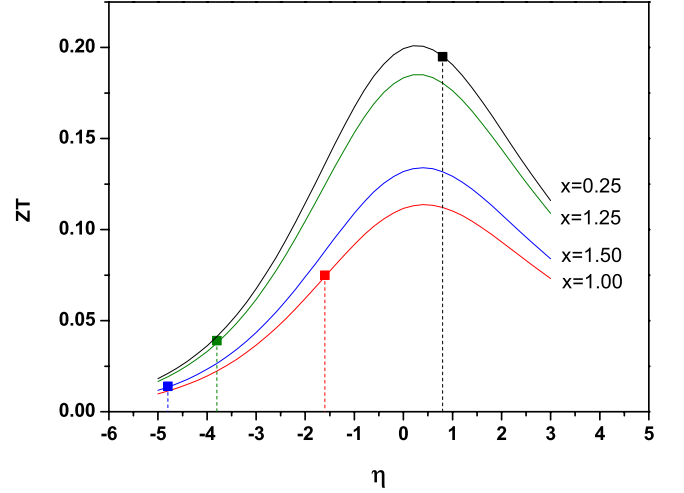

FIG. 9. (Color online) Calculated theoretical dependences (lines) and experimental values (markers) of ZT parameter on reduced Fermi energy η for selected compositions x of $AgSbSe_xTe_{2-x}$ materials ($T=300$ K).

elements or compounds, as a result of enhanced mass and volume fluctuations. This effect is also observed in the case of $AgSbSe_xTe_{2-x}$ solid solutions. The lowest thermal conductivity of 0.48 W m^{-1} K^{-1} has the sample with nominal composition of $AgSbSeTe$ ($x=1$). However, the effect of alloying on reduction of total thermal conductivity is lower than in typical binary systems. A rather weak influence of alloying can be a consequence of extremely low heat transport in $AgSbSe_2$ and $AgSbTe_2$ base compounds. Morelli *et al.*[23] showed that experimental lattice-thermal conductivity λ of $AgSbTe_2$ is in excellent agreement with estimated theoretical minimum $\lambda_{\min} \approx 0.6$ W m^{-1} K^{-1} at 300 K for assumed phonon mean-free path l equal to the interatomic distance in this compound ($d=0.303$ nm). Therefore, also in case of isostructural solid solutions of this compound their thermal conductivity cannot be significantly lower.

D. Estimation of *ZT* parameter

Obtained experimental data allow calculating dimensionless thermoelectric figure of merit ZT for our materials. Using Eq. (1) we have determined temperature dependence on ZT parameter. Figure 8 presents results for selected materials.

The highest experimental figure of merit $ZT=0.65$ has the sample with composition of $AgSbSe_{0.25}Te_{1.75}$ at the temperature of 520 K. It can be noticed that in general, single-phased solid solutions exhibit lower ZT values than heterogeneous samples, despite their very high Seebeck coefficient α and low thermal conductivity λ. Relatively low ZT values are the consequence of too low electrical conductivity σ resulting from nonoptimal concentration of current carries in these materials. An increase in carrier concentration usually leads to the increase in both electrical σ and thermal conductivity λ and simultaneous decrease in thermopower values α. For particular carriers concentration n_{opt} the term $\alpha^2\sigma\lambda^{-1}$ in Eq. (1) reaches maximum.

Optimal transport parameters (e.g., α, σ, L) as well as carrier concentration n_{opt} can be estimated using a methodology developed by Chasmar and Stratton.[26] According to their approach, ZT parameter for a general case of both degenerated and nondegenerated semiconductors can be expressed in the form

$$ZT = \left(\frac{ea}{k_B}\right)^2\left[\frac{\sigma_0}{\sigma\beta} + \left(\frac{e}{k_B}\right)^2 L\right]^{-1}, \qquad (7)$$

where σ_0 and β are defined as follows:

$$\sigma_0 = 2e\mu\left(\frac{2\pi m^*k_BT}{h^2}\right)^{3/2} \qquad (8)$$

and

$$\beta = \left(\frac{k_B}{e}\right)^2\frac{\sigma_0 T}{\lambda_{latt.}} = 5,745 \cdot 10^{-6}\frac{\mu}{\lambda_{latt.}}\left(\frac{m^*}{m_0}\right)^{3/2}T^{5/2}. \qquad (9)$$

Transport parameters can be expressed as functions of reduced Fermi energy η Eqs. (2)–(5) as well as electrical conductivity σ

$$\sigma = \sigma_0\frac{F_r(\eta)}{\Gamma(r+3/2)}, \qquad (10)$$

where Γ is the Euler's gamma function.

Given the above dependences and experimental values of $\alpha, \sigma, \mu, \lambda_{latt.}$, and m^*, and ZT parameter can be estimated as a function of reduced Fermi level η for the given temperature. For the determination of Fermi level η_{exp} corresponding to experimental ZT values we have used Seebeck coefficient data in Eq. (2). Alike in previous calculations, we assumed $r=-\frac{1}{2}$ which is the appropriate value for either acoustic-mode lattice scattering or alloy scattering.

Figure 9 shows the results of computations and experimental ZT for selected materials: both homogeneous samples ($x>1$) as well as for the heterogeneous sample ($x=0.25$) with the highest experimental ZT value at 300 K. The maxi-

mum value ZT_{max} for model curves corresponds to the Fermi energies η_{opt} close to zero which is a typical case for most of thermoelectric materials. The determined optimal values α_{opt}, corresponding for ZT_{max}, are between 180 and 195 μV K^{-1} and carriers concentration n_{opt} of about 1.7×10^{18} cm^{-3} in all samples.

The above results show that thermoelectric figure of merit of homogeneous alloys can be significantly improved (even two to five times) by careful p-type doping. An increase in holes concentration to the amount of n_{opt} should move the Fermi energy E_f to the optimum position near the valence-band edge. In the case of the heterogeneous sample (x =0.25) its ZT value at the room temperature is close to the maximum and probably cannot be significantly suppressed by changing the concentration of current carriers.

It should be noted that above estimations were made with many simplified assumptions such as the simple band-structure model, constant scattering factors, and rigid-band behavior taken into account; hence, the obtained values of thermoelectric figure of merit can be underestimated. For example, in complex band structures the ZT parameter can be higher than in the simple single-band case due to higher DOS near the Fermi energy.[9] Therefore, precise prediction of the influence of impurity on thermoelectric properties requires more advanced theoretical attempts including electronic-structure computations for each particular case.

IV. CONCLUSIONS

The structural and transport properties in AgSbTe$_2$-AgSbSe$_2$ system from RT to 520 K were studied. Samples with predominant amount of AgSbTe$_2$ have heterogeneous composition. The remaining materials with excess of AgSbSe$_2$ are single-phased solid solutions of stable NaCl crystal structure in the wide temperature range. All samples are p type with hole concentration between $10^{16}/10^{19}$ cm^{-3}. Homogeneous alloys of AgSbTe$_2$-AgSbSe$_2$ exhibit apparent semiconducting behavior ($E_g \sim 0.3/0.4$ eV) in contrary to base compounds and heterogeneous materials which seem to have much narrower band-gap or semimetallic properties. The band-gap width E_g in homogeneous alloys strongly depends on chemical composition, so manipulation of Te/Se ratio allows tuning this parameter to required value. Despite that thermal conductivity of AgSbTe$_2$ is close to the minimal theoretical value λ_{min}, alloying with AgSbSe$_2$ leads to further decrease in heat conduction to 0.48 W m^{-1} K^{-1}.

Received materials exhibit very promising initial thermoelectric properties. The highest experimental value of ZT is about 0.65 at temperature of 520 K for the sample with nominal composition of AgSbSe$_{0.25}$Te$_{1.75}$. However, theoretical estimations show that this parameter in homogeneous samples can be much elevated in higher temperatures if the concentration of current carriers is optimized.

*Corresponding author; gcwojcie@cyf-kr.edu.pl

[1] S. Geller and J. H. Wernick, Acta Crystallogr. **12**, 46 (1959).

[2] J. H. Wernick and K. E. Benson, Phys. Chem. Solids **3**, 157 (1957).

[3] R. Wolfe, J. H. Wernick, and E. Haszko, J. Appl. Phys. **31**, 1959 (1960).

[4] K. Wang, C. Steimer, R. Detemple, D. Wamwangi, and M. Wuttig, Appl. Phys. A **81**, 1601 (2005).

[5] J. Xu, B. Liu, Z. Song, S. Feng, and B. Chen, Mater. Sci. Eng., B **127**, 228 (2006).

[6] A. R. Patel and D. Lakshminarayana, Thin Solid Films **98**, 59 (1982).

[7] A. Abdelghany, S. N. Elsayed, D. M. Abdelwahab, A. H. Abou El Ela, and N. H. Mousa, Mater. Chem. Phys. **44**, 277 (1996).

[8] A. R. Patel, D. Lakshminarayana, and K. V. Rao, Thin Solid Films **98**, 51 (1982).

[9] *Handbook of Thermoelectrics*, edited by D. M. Rowe (CRC, Boca Raton, FL, 1994).

[10] K. F. Hsu, S. Loo, F. Guo, W. Chen, J. S. Dyck, C. Uher, T. Hogan, E. K. Polychroniadis, and M. G. Kanatzidis, Science **303**, 818 (2004).

[11] N. Chen, F. Gascoin, G. J. Snyder, E. Müller, G. Karpinski, and C. Stiewe, Appl. Phys. Lett. **87**, 171903 (2005).

[12] J. P. McHugh, W. A. Tiller, S. E. Haszko, and J. H. Wernick, J. Appl. Phys. **32**, 1785 (1961).

[13] R. W. Armstrong, J. W. Faust, and W. A. Tiller, J. Appl. Phys. **31**, 1954 (1960).

[14] R. A. Burmeister and D. A. Stevenson, Trans. Metall. Soc. AIME **230**, 329 (1964).

[15] R. M. Marin-Ayral, B. Legendare, G. Brun, B. Liautard, and J. C. Tedenac, Thermochim. Acta **131**, 37 (1988).

[16] R. Marin, G. Brun, and J. C. Tedenac, J. Mater. Sci. **20**, 730 (1985).

[17] R. Marin, G. Brun, M. Maurin, and C. Tedenac, Eur. J. Solid State Inorg. Chem. **27**, 47 (1990).

[18] H. Ma, T. Su, P. Zhu, J. Guo, and X. Jia, J. Alloys Compd. **454**, 415 (2008).

[19] G. Petzow and G. Effenberg, *Ternary Alloys* (Wiley-VCH Verlag, Weinheim, 1988), Vol. 2, p. 554.

[20] K. Wojciechowski, J. Tobola, M. Schmidt, and R. Zybala, Fifth European Conference on Thermoelectrics, Odessa, Ukraine, 2007, p. 117–121.

[21] K. T. Wojciechowski, J. Tobola, M. Schmidt, and R. Zybala, J. Phys. Chem. Solids **69**, 2748 (2008).

[22] K. Hoang, S. D. Mahanti, J. R. Salvador, and M. G. Kanatzidis, Phys. Rev. Lett. **99**, 156403 (2007).

[23] D. T. Morelli, V. Jovovic, and J. P. Heremans, Phys. Rev. Lett. **101**, 035901 (2008).

[24] V. Jovovic and J. P. Heremans, Phys. Rev. B **77**, 245204 (2008).

[25] R. S. Kumar, A. Sekar, N. Victor Jaya, and S. Natarajan, J. Alloys Compd. **285**, 48 (1999).

[26] R. P. Chasmar and R. J. Stratton, J. Electron. Control **7**, 1578 (1959).